RESILIENT INFRASTRUCTURE
June 1–4, 2016
RESILIENT INFRASTRUCTURE LONDON 2016

MONITORING THE CORROSION PROCESS OF REINFORCED CONCRETE FLAT SLAB-COLUMN CONNECTION

Mahmoud, E. Said,
Memorial University, Canada

Amgad Hussein,
Memorial University, Canada

Assem A. Hassan,
Memorial University, Canada

ABSTRACT

The corrosion of the steel reinforcement embedded in a two-way reinforced concrete flat slab around the column stub area was investigated in this study, which aimed to studying the effect of corrosion on the shear punching behavior. Two square flat slab-column connections were cast, the flat slab dimension was 1900 mm × 1900 mm × 150 mm, and the column dimensions was 250 mm × 250 mm. A specific delaminated area was corroded around the column stub to emphasize the effect of corrosion around punching area. The corrosion reached two levels of mass loss uniformly over that specified area: 0% and 26%. Corrosion process was monitored under an accelerated corrosion technique through the application of a constant potential of fifteen volts to reach the targeted uniform corrosion level. Then, the corrode slab-column connection was loaded until failure for each slab occurred. The corrosion performance of the slab was evaluated based on the results of the current measurement, half-cell potential tests, and mass loss. The test results show that the corrosion of reinforcement rebar around the column stub in flat slab causes a significant loss in punching shear capacity and affects the structural integrity by increasing crack widths.

Keywords: Corrosion, Flat slab, Punching, Structural integrity, Crack width.

1. INTRODUCTION

The deterioration of reinforced concrete structures due to reinforcement corrosion is a serious problem that faces the concrete industry worldwide. Corrosion is an electrochemical reaction between steel reinforcement and the surrounding environment that has convenient amount of chloride. Chloride ions penetrate and diffuse through the concrete cover reaching the embedded steel reinforcement and thus causing corrosion. The corrosion of steel reinforcement causes a reduction in the capacity of the structure. In addition, cracks area created in the concrete cover from the products of corrosion. Thus, the safety and the serviceability of the corroded structures are reduced (Neville 2011).

Reinforced concrete flat slabs are commonly used in parking garage structures. Parking structures are one of the most structures that are exposed directly to harsh environmental conditions, especially in cold climates such as Canada. Parking garage structures are usually exposed to water, snow, ice, and de-icing salts which increase the probability of corrosion of the top flexural reinforcement. The most vulnerable structural element that can be affected by corrosion in the parking structures is the slab-column connection, which could fail due to punching shear (Reilly et al. 2014). There are several existing structures that collapsed due to punching shear failure such as a parking garage collapse in Bluche, Switzerland, in 1981 (Mirzaei 2008); and a parking garage collapse in Ville St. Laurent, Québec in 2008 (Reilly et al. 2014).

The punching shear failure of slab-column connections has been investigated by many researchers. However, little research was carried out to examine the effect of corrosion on the punching shear. Rahman (1992) studied the effect

of corrosion on the slab-column connection. He simulated the effect of corrosion by decreasing the number of top flexural bars and using empty sheathes as broken tendons. The researcher concluded that 50% loss in bar and tendon area reduced the punching shear capacity by 30%. He also examined the effect of loss of bond and concrete delamination. The author simulated the loss of bond by wrapping the reinforcing bars with adhesive plastic tape. The delamination was simulated by placing a polyethylene sheet between the upper and lower layers of the top reinforcing mat. Deflections and crack widths were more noticeable due to loss of bond and delamination. However, the punching load capacities in both cases increased slightly, which is obviously in contrast to what might be expected

Aoude et al. (2014) simulated delamination of two-way slab column connections. The delamination was simulated by placing a plastic sheet under the flexural reinforcement. Four different specimens were tested: a control specimen with no delamination, a specimen simulating a slight delamination by extending this plastic sheet for a short distance around the column, a specimen simulating medium delamination by using the plastic sheet with dimension such that the flexural reinforcement had a remaining embedment length at the edges of the specimen equal to the development length, L_d, and a specimen simulating a large degree of delamination by using a plastic sheet allowing only $0.5L_d$ of the flexural reinforcement to remain bonded. The authors concluded that slight delamination caused a 4% increase in the punching shear capacity; medium delamination caused only a 3% decrease in the punching shear capacity; and severe delamination caused a 12% reduction in punching shear capacity.

Reilly et al. (2014) studied the effect of large delamination on the punching and post-punching responses of slab-column connections using the same technique as Aoude et al. (2014). The authors concluded that severe delamination of the flexural reinforcement lead to decrease in the pre-punching stiffness, punching shear resistance, and post-punching shear resistance of the specimens. They also concluded that well design of structural integrity reinforcement enhanced post-punching shear resisting mechanism, where it caused increasing the post-punching shear resistances and ultimate deflections (Reilly et al. 2014).

This study investigates the effects of real corrosion of the reinforcement on the punching responses of slab-column connections in parking structures. An accelerated corrosion technique was used by applying a constant voltage between the outside stainless steel nets (cathode) and the embedded reinforcement steel (anode) using a DC power source in presence of electrolyte solution. This acceleration technique was used before in several experiments on beams (Hassan et al. 2010; Hassan et al. 2009). This is the first research that used this technique in flat slab-column connections.

2. EXPERIMENTAL PROGRAM

This paper investigates the effect of corrosion performance on flat slab-column connections. Using accelerated corrosion technique to reach the targeted uniform corrosion level. The corrosion performance of the slab was evaluated based on the results of the current measurement, half-cell potential tests, and mass loss. The test results were showed in terms of deflection profiles, load-deflection response, punching shear resistance, load vs. crack width curve, crack pattern, and concrete strain profile.

2.1 Details of Test Specimens

Two reinforced concrete flat slab-column connection were cast. Each specimen had dimension of 1900x1900x150 mm and consisted of 250 mm column stub extending 200 mm. The clear cover was 30mm. The main reinforcement was 1% reinforcement ratio, distributed uniformly using 15M bar [db = 16 mm] (see Figure 1). The details of the test specimens are showed in Table 1. The slab-column connections designation included a combination of letters and numbers: C0 and C26 to indicate the level of corrosion, where C0 refers to a 0% level of corrosion while C26 refers to 26% level of corrosion.

Table 1: Details of Slab Specimens

Specimens	Properties	C mm	d mm	f_c' MPa	Main reinforcement	Delaminated area mm x mm
C0	Control (0 % corrosion)	250	104	40	Two layers of 15M bars with $\rho = 1\%$	N/a
C26	Corroded (26 % corrosion)	250	104	40	Two layers of 15M bars with $\rho = 1\%$	70x70

* C is column width, d is the effective slab depth, ρ reinforcement ratio, f_c' is concrete compressive strength

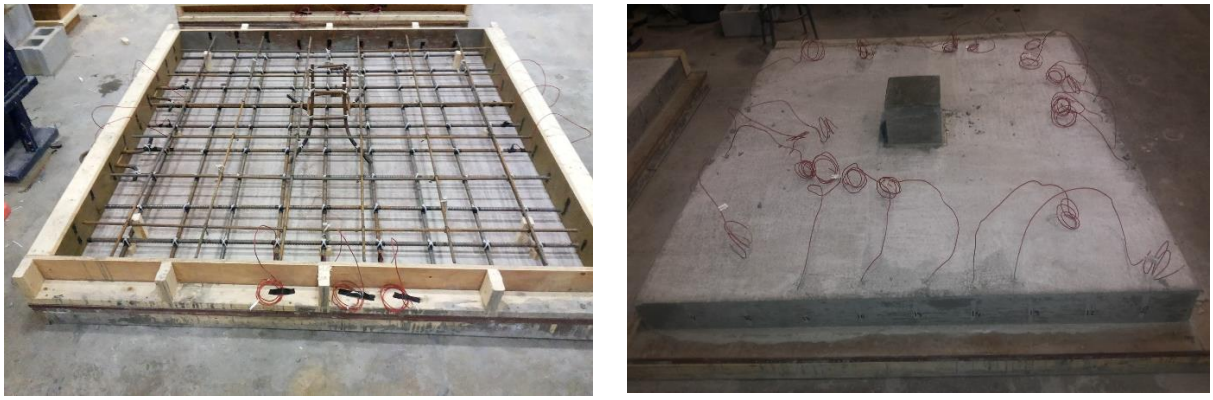

(a) (b)

Figure 1: Typical slab specimens: (a) before casting; (b) after casting

2.2 Material Properties

The mixes for the two flat slab-connection were the same to achieve the same compressive strength 40 MPa. Table 2 shows the mix composition of the concrete mixture used in casting the two specimens. The targeted compressive strength and the water to cement ration (w/c) were chosen according to ACI specification to consider the type of exposure for the case of parking garage structures (case F3). ACI recommendation for case F3; compressive strength not less than 35MPa, and w/c ration not more than 0.4 (ACI Committe-318 2014). The concrete is delivered through a ready mix. Table 3 illustrates the material properties of the Grade 400 Mpa 15M reinforced bars used in the slab specimens. It also shows the material properties of the concrete that used for casting the two slabs.

Table 2: Concrete mixture composition for 1 m^3

Cement (kg)	Water/cement ratio	Water (L)	Coarse/Fine ratio	Coarse Aggregate (kg)	Fine Aggregate (kg)	Aggregate size (mm)
350	0.4	140	1.3	1083	833	10

Table 3: Steel and concrete properties

Slab	Steel properties				Concrete Properties			
	Designation	Area mm^2	f_y MPa	$\mu\varepsilon_y$	f_c' MPa	Measured f_r MPa	Calculated f_r MPa	$\frac{f_r}{\sqrt{f_c'}}$
C0 C26	15M	200	443	2200	40	3.815	3.79	0.603

* f_y is steel yield strength, ε_y is steel strain, f_c' is concrete compressive strength, f_r is modulus of rupture

2.3 Casting of Slab-Column Connections

The concrete mixture was delivered to Memorial University Structure Laboratory in a truck by a ready mix. Directly after the concrete had been dispatched, the slump was measured, cylinders and prisms were filled with the delivered concrete, and the slabs were cast in prepared wooden forms. Electrical vibrator was used to consolidate the concrete, and the top surface was smoothed using finishing trowels. The column stub was cast after twenty-four hours from casting the flat slabs. After a day from casting the column stub, the frameworks were removed and the slabs were moist-cured for four days, then air curried until the date of testing for C0 and the date of starting the accelerated corrosion for C26.

2.4 Accelerated Corrosion Setup

Accelerated corrosion technique has been used before in previous tests showing a reasonable results about the sensitivity of steel reinforcement to the corrosion (Amleh & Mirza 2000). The accelerated corrosion setup used in this investigation consisted of electrolytic solution (5% sodium chloride (NaCl) by the weight of the water) and steel mesh placed at the top of the slab over the targeted corroded area. Foam sheets were used to construct a tank above the targeted corroded area. The foam tank is immersed with the electrolytic solution as shown in Figure 2. To avoid any change in the concentration of the sodium chloride in the electrolyte solution, the solution was permuted every week. A direct current with constant volt of 15V was applied to the slab, where the steel reinforced bars under the targeted corroded area served as anodes while the steel mesh served as a cathode. A data-acquisition system was used to record the current flow from anode to cathode as shown in Figure 3. The theoretical mass loss is calculated based on Faraday's equation as shown in Eq. (1):

$$[1] \qquad \text{Mass loss} = \frac{t \,.i \,.M}{z \,.F}$$

Where t = the time passed in seconds, i = the current passed in amperes, M = atomic weight (for iron M = 55.847 g/mol), z = ion charge (two moles of electrons) and F = Faraday's constant which is the amount of electrical charge in one mole of electron (F=96,487) (Hassan et al. 2009).

2.5 Half-Cell Potential Measurements

ASTM has been adopted the half-cell potential technique as an indication of corrosion in 1977 (ASTM C876 1999). This method measures the electrochemical potential of reinforcement against a reference placed on the concrete surface. The reading measurement give an indication of the probability of corrosion, if the readings are more negative values imply a bigger chance for the occurrence of corrosion while positive values imply a very low chance for the occurrence of corrosion. Half-cell potential measurements were taken periodically at twenty-four different points the cover the corroded area. The corroded area was chosen to cover the critical punching area that was taken as 1.5 depth of the slab from the face of the column, according to BS8110 (BS 8110 1997; British Standards Institution 2004) as shown in Figure 4. The reading of half-cell was taken every 3 days.

2.6 Measurement of Mass Loss

After the slab C26 corroded and the measurement of half-cell and crack widths were recorded, the slab-column connection was jackhammered using demolition hammer to remove the corroded longitudinal reinforcement bars. The rust and all adhered corroded products on the corroded bars were cleaned using a wire brush, then the bars soaked in a HCL solution according to ASTM Standards G1-03 method (ASTM G1-03 2003). After that the cleaned bars were weighted and the percentage mass loss for each bar was calculated based on Eq. (2):

$$[2] \qquad \%\ \text{mass loss} = \frac{(\text{initial weight} - \text{final weight})}{\text{initial weight}} \text{ x } 100$$

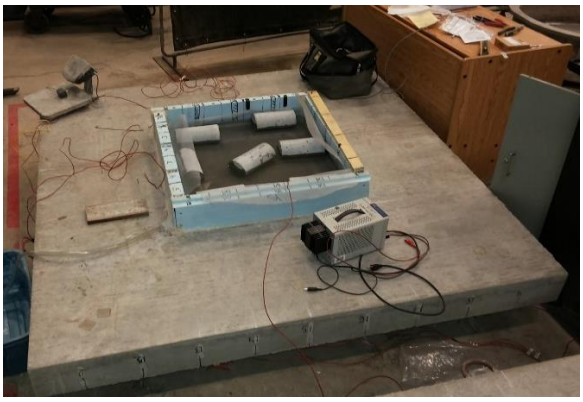

Figure 2: Corrosion setup above the targeted corroded area

Figure 3: Corrosion current monitoring by data-acquisition system

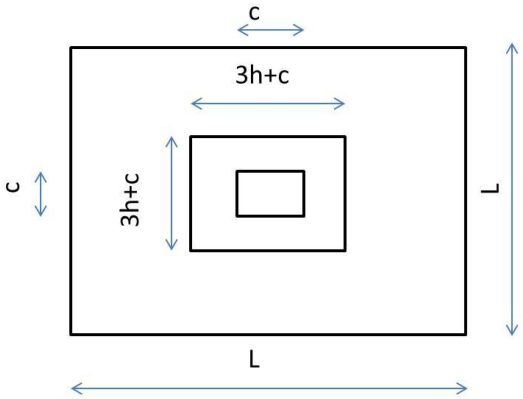

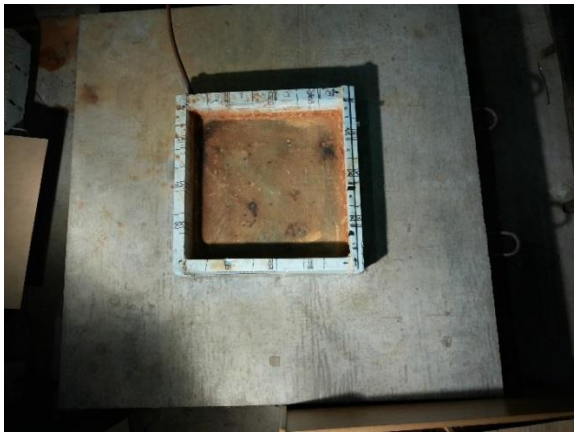

Figure 4: Illustrates the targeted delaminated corroded area

3. EXPERIMENTAL RESULTS AND ANALYSIS

3.1 General Cracking Observation

Figure 5 shows the crack pattern for the corroded specimen C26 after the completion of the corrosion process. C26 had had a maximum crack width of 0.5 mm before doing the punching test. Figure 6 illustrates the crack width verses the level of corrosion for C26. It can be noted that the rate of widening the crack width was increased with increasing the level of corrosion. This widening can be attributed to the enlargement of the corrosion products around the steel bar with increasing the level of corrosion, which exerted pressure on the concrete cover. Those cracks due to corrosion had contributed on changing the behavior of the crack distribution during the punching test on C26 comparing with C0. Figure 7 shows that C26 had a radial crack pattern distribution after the punching test while C0 had an orthogonal crack pattern distribution. In addition, the maximum crack width for C26 at the end of the test was 7.93 mm while at C0 it was 2.49 mm. This results can be interrupted to the fact that the initiated cracks at C26 is bigger than the pre-cracking of C0 by 0.48 mm, a pre-cracking was done for C0 before punching test. This big difference in crack width also had effected the punching radius; C0 has a big punching radius while C26 had a small punching radius bounded around the corroded area as shown in Figure 7. That reason beside the point of reducing mass loss of steel reinforcement have influence on the punching capacity for C26 which was reduced by 20% comparing with C0.

Figure 5: Corrosion-Cracked patteren on the corroded area

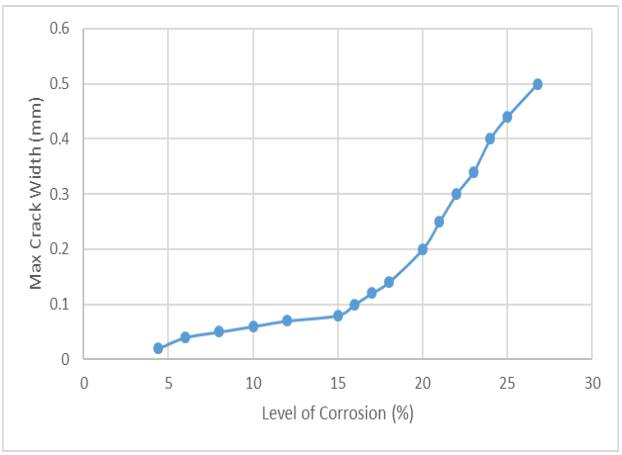

Figure 6: Maximum Crack with level of corrosion

(a)

(b)

Figure 7: Crack Pattern in |Specimen: (a) C0; (b) C26

3.2 Time-dependent corrosion tests results

3.2.1 Current Results

The rate of corrosion was monitored and recorded during the acceleration corrosion test by a computer-controlled data-acquisition system. Figure 8 shows the relation between the current and the immersion time. It can be noted that the current was initially dropped down followed by genteelly increased till 14% of mass loss then the current rate was gradually increased till the targeted level of corrosion 26% of mass loss. The current dropped down in the first few days is an implication of creation of the passive film around the steel reinforcement, which prevents reinforcement against corrosion. When this passivation layer become weaken due to the ingress of chlorides, the corrosion starts and the corrosion rate increases progressively (ASTM C876 1999). The sudden jump in the current verses time might me caused due to losing the bond between the concrete cover and steel reinforcement and due to starting spalling for the concrete cover (Hassan et al. 2009). Figure 9 shows the mass loss rate with time. Its noted that the rate of losing mass is increased when the current rate increased, which associated with increasing in the rate of corrosion.

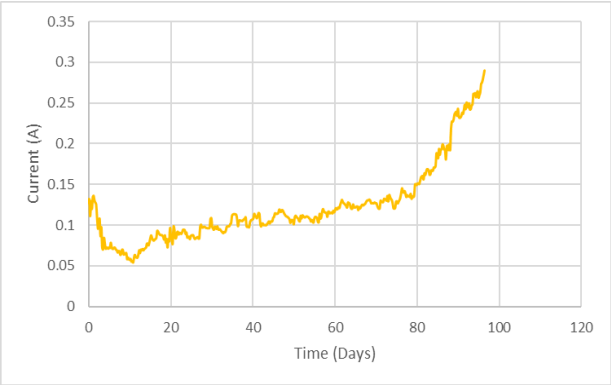

Figure 8: Current time history for C26 specimen

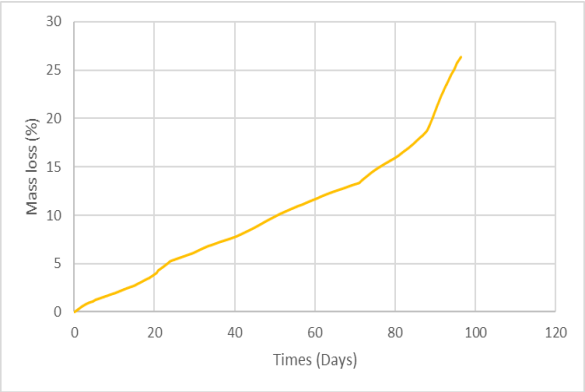

Figure 9: Mass loss rate with time

3.2.2 Half-Cell Potential Measurements

Figure 10 illustrates the variation of half-cell potential readings over the corroded area with age. The potential reading was measured above each corroded steel reinforcement bar for the top reinforcement mesh. Figure 11 shows the variation of half-cell potential reading verses the level of corrosion. It can be noted from the both figures that the steel bars near the concrete cover give more negative values than the steel bars that are farther, second layer of the steel mesh. The more negative values are an indication of the higher probability of corrosion; the upper bars had bigger probability to corrode faster than the lower steel bars at the top mesh. This was expected because the upper layer of steel mesh had a clear concrete cover of 30mm while the lower layer for the steel mesh had a clear concrete cover of 46mm. Therefore, the upper steel bars were more subjected to chlorides ingress more than the lower one for the top steel mesh. This result was conducted with other researchers that the concrete cover has a big influence in the half-cell potential reading (Klinghoffer 1995). The figures also show that the reading of the half-cell potential test did not give variation in reading when corrosion really occurred; therefore, the half-cell potential test only be used to represent the probability of corrosion for un-corroded slabs, but when corrosion happens it may not give any indication for the level of corrosion.

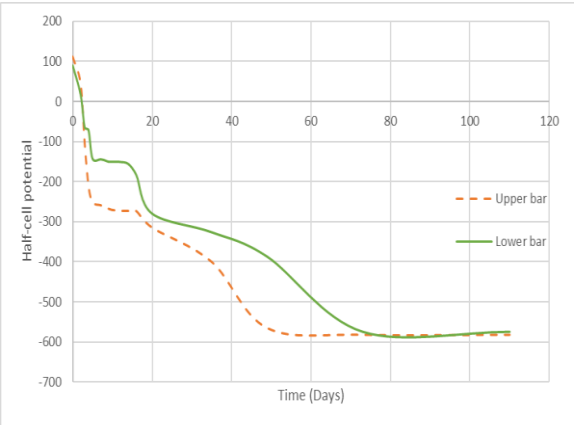

Figure 10: Half-cell potential reading vs. age

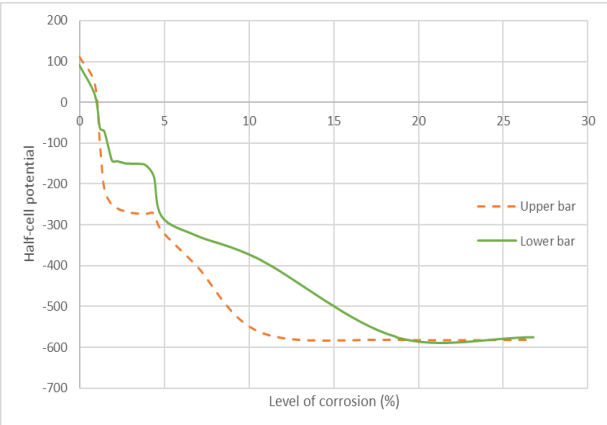

Figure 11: Half-cell potential reading vs. level of corrosion

3.3 Test Results After Corrosion

3.3.1 Mass Loss

The theoretical mass loss was calculated using Faraday's Eq. (1), this equation is based on the amount of the current that passed across the steel bar. After the punching test had been done, a demolition for the slab-column connection had been occurred using a demolition hammer to extract the corroded bars as shown in Figure 12. The actual mass loss for the corroded bars found to be little bit less than the actual mass loss. The Faraday's equation gives a good relation between actual and predicted mass loss when the current passes through a bar suspended in salt solution. In another hand, when the current passes through embedded bars inside concrete, the theoretical mass loss overestimates the actual mass. This overestimates might be related to losing of some current through concrete cover to reach the embedded the steel reinforcement, which do not contribute on the corrosion (Spainhour & Wootton 2008; Auyeung et al. 2000).
It was observed during the demolition of the slab that the corroded area was easy to destroy comparing with the un-corroded area that was very hard to destroy it. This observation indicates that the bond was diminished under the corroded area and a delamination started to happened as shown in Figure 13. This delamination part effects the punching shear area of C26 comparing with C0 as mentioned in section (3.1).

Figure 12: Corroded bars after demolition process

Figure 13: Delamination area around the corroded region

4. CONCLUSION

The corrosion performance and cracking behavior of flat slab-column connection were investigated based on a real corrosion process using the accelerated corrosion technique. Based on the results presented in this paper, the following conclusions were warranted:

- The cracks performance during the punching test in the un-corroded specimen C0 was easily propagated and extended while in the corroded specimen C26 the cracks did not propagate as much as C0. This is can be attributed to the initial crack widths at C26 were bigger than C0, therefore during loading the cracks at C26 specimen become widen while new cracks initiated and propagated at C0.
- The crack width can be used as indication for the corrosion with associating of the half-cell potential readings. When the reading of half-cell potential around the crack gives more negative values that are an indication of the higher probability of corrosion. When the level of corrosion increases, the accumulated corrosion products increases around the steel bars which increases the pressure beneath the concrete cover, leading to widening the crack widths. However, the development of accurate relationships between crack width and level of corrosion needs more experimental data for slabs with different concrete covers and different corrosion levels.
- The corrosion products causing delamination only under the corroded area, leading to minimizing the punching radius at C26 comparing with C0 and leading to decrease the punching resistance.
- The predicted mass loss using Faraday's equation has a strong estimation for the actual mass loss in the corroded flat slab-column connection. Therefore, the theoretical mass loss estimation can be used to examine the effect of corrosion over time.
- The results indicate that the corrosion of steel reinforcement reduces the punching shear capacity in C26 by 20% comparing with the control specimen C0.

5. REFERENCES

A.Neville, 2011. *Properties of concrete (fourth edition)*.

ACI Committe-318, 2014. *Building Code Requirement for Structural Concrete (ACI 318M-14) and Commentary (ACI 318RM-14)*,

Amleh, L. and Mirza, M.S., 2000. *Bond deterioration of reinforcing steel in concrete due to corrosion*.

Aoude, H., Cook, W.D. and Mitchell, D., 2014. Effects of Simulated Corrosion and Delamination on Response of Two-Way Slabs. *Journal of structural Engineering*, 140(1), pp.1–9.

ASTM C876, 1999. *Standard Test Method for Half-Cell Potentials of Uncoated Reinforcing Steel in Concrete*,

ASTM G1-03, 2003. *ASTM G1 Standard Practice for Preparing, Cleaning, and Evaluation Corrosion Test Specimens*,

Auyeung, Y., Balaguru, P. and Chung, L., 2000. Bond behavior of corroded reinforcement bars. *Materials Journal*, 97(2), pp.214–220.

British Standards Institution, 2004. *Eurocode 2: Design of Concrete Structures: Part 1-1: General Rules and Rules for Buildings*, British Standards Institution.

BS 8110, 1997. Structural use of concrete. Part I: Code of practice for design and construction. *British Standards Institution, UK*.

Hassan, A.A.A., Hossain, K.M.A. and Lachemi, M., 2009. Corrosion resistance of self-consolidating concrete in full-scale reinforced beams. *Cement and Concrete Composites*, 31(1), pp.29–38. Available at: http://dx.doi.org/10.1016/j.cemconcomp.2008.10.005.

Hassan, A.A.A., Hossain, K.M.A. and Lachemi, M., 2010. Structural assessment of corroded self-consolidating concrete beams. *Engineering Structures*, 32(3), pp.874–885. Available at: http://linkinghub.elsevier.com/retrieve/pii/S0141029609003976 [Accessed December 29, 2014].

Klinghoffer, O., 1995. In situ monitoring of reinforcement corrosion by means of electrochemical methods. *Nordic Concrete Research-Publications-*, 95(1), pp.1–13. Available at: http://www.germann.org/Publications/GalvaPulse/2. Klinghofer, O., In Situ Monitoring of Reinforcement Corrosion by means of Electrochemical Methods, Nordic Concrete Research 95 1.pdf.

Kuang, J.S. and Morley, C.T., 1993. Punching Shear Behavior of Restrained Reinforced Concrete Slabs. *ACI Structural Journal*, 89(1), pp.13–19.

Mirzaei, Y., 2008. Post punching behavior of reinforced slab-column connections. *7th Int. FIB Ph.D. Symp., IWB Universität Stuttgart, Stuttgart.*, pp.1–8.

Rahman, A.H., 1992. *Effect of steel corrosion on the strength of slab-column connections*, National Research Council Canada, Institute for Research in Construction.

Reilly, J.L. Cook, William D., Bastien, J. and Mitchell, D., 2014. Effects of Delamination on the Performance of Two-Way Reinforced Concrete Slabs. *Journal of Performance of Constructed Facilities*, 28(4), pp.1–8.

Spainhour, L.K. and Wootton, I.A., 2008. Corrosion process and abatement in reinforced concrete wrapped by fiber reinforced polymer. *Cement and Concrete Composites*, 30(6), pp.535–543.